

Effects of metal enrichment and metal cooling in galaxy growth and cosmic star formation history

Jun-Hwan Choi^{*}, Kentaro Nagamine[†]

Department of Physics & Astronomy, University of Nevada, Las Vegas, 4505 S. Maryland Pkwy, Las Vegas, NV, 89154-4002, U.S.A.

26 October 2018

ABSTRACT

We present the results of a numerical study on the effects of metal enrichment and metal cooling on galaxy formation and cosmic star formation (SF) history using cosmological hydrodynamic simulations. We find following differences in the simulation with metal cooling when compared to the run without it: (1) the cosmic star formation rate (SFR) is enhanced by about 50 & 20% at $z = 1$ & 3, respectively; (2) the gas mass fraction in galaxies is lower; (3) the total baryonic mass function (gas + star) at $z = 3$ does not differ significantly, but shows an increase in the number of relatively massive galaxies at $z = 1$; (4) the baryonic mass fraction of intergalactic medium (IGM) is reduced at $z < 3$ due to more efficient cooling and gas accretion onto galaxies. Our results suggest that the metal cooling enhances the galaxy growth by two different mechanisms: (1) increase of SF efficiency in the local interstellar medium (ISM), and (2) increase of IGM accretion onto galaxies. The former process is effective throughout most of the cosmic history, while the latter is effective only at $z < 3$ when the IGM is sufficiently enriched by metals owing to feedback.

Key words: method : numerical — galaxies : evolution — galaxies : formation — galaxies : high redshift — galaxies : mass function — cosmology : theory

1 INTRODUCTION

Gas cooling plays a key role in galaxy formation. According to the hierarchical structure formation model, galaxies form in gravitationally collapsed dark matter halos. The dissipative baryonic matter cools by emitting radiation and condenses into halos to form galaxies (Rees & Ostriker 1977; White & Rees 1978). Subsequently stars form through the radiative cooling of interstellar medium (ISM; e.g., McKee & Ostriker 2007).

The cooling rate of gas varies with its chemical abundance, because different atoms and molecules have different cooling rates. The chemical abundance of cosmic gas evolves as a function of time and environment. In the early universe, the primordial gas consists of mainly hydrogen (mass fraction of $X \simeq 0.74$) and helium (mass fraction of $Y \simeq 0.25$) with a negligible amount of light metals (e.g. Burles et al. 2001). Throughout this paper, all the elements heavier than helium are collectively called ‘metals’. Most metals are produced inside stars and spread out to the space by galactic

winds driven by supernova (SN) explosions. In the metal-enriched gas, the total cooling rate is significantly enhanced relative to that of the primordial gas by the atomic emission lines from recombination of ionised metals.

Metals may influence galaxy formation in two different ways. Firstly, the SF efficiency is increased owing to the shorter gas cooling time. Star formation generally takes place in dusty metal-enriched ISM, therefore, the enhanced cooling rate by metals would boost up the SF efficiency. However, the energy/momentum feedback by SNe may suppress the subsequent star formation after the initial starburst by heating up the ambient gas. This complicates the situation, and it is not clear whether the net effect of metal cooling and SN feedback would be negative or positive. The feedback process is highly nonlinear, therefore, a direct numerical simulation would be a useful tool to explore the effects of feedback and metal cooling.

Secondly, the metals dispersed into the IGM by SN feedback also enhance the cooling of IGM. This can lead to the increase of IGM accretion onto galaxies, because colder gas can sink into galaxies more easily. Both of the above two effects may affect the galaxy growth and cosmic SF history significantly. Therefore it is essential to include the effects of metal cooling and chemical enrichment by feedback in the studies of galaxy formation and evolution, and capture the

^{*} Email: jhchoi@physics.unlv.edu

[†] Visiting Researcher, Institute for the Physics and Mathematics of the Universe, University of Tokyo, 5-1-5 Kashiwanoha Kashiwa-shi, Chiba 277-8582 Japan

complex two-way interactions between galaxies and IGM. In addition, metal enrichment also affects the equation of state by altering the mean molecular weight of gas, which influences the hydrodynamic calculation of gas thermal state.

Cosmological hydrodynamic simulations are widely used in the studies of galaxy formation and cosmic SF history (e.g., Cen 1992; Katz et al. 1992; Cen & Ostriker 1993; Katz et al. 1996; Nagamine et al. 2000; Pearce et al. 2001; Nagamine et al. 2001a,b; Ascasibar et al. 2002; Murali et al. 2002; Nagamine 2002; Weinberg et al. 2002; Kawata & Gibson 2003; Kravtsov 2003; Marri & White 2003; Springel & Hernquist 2003b; Governato et al. 2004; Robertson et al. 2004; Weinberg et al. 2004; Nagamine et al. 2004, 2005a,b; Cen et al. 2005; Kereš et al. 2005; Finlator et al. 2006; Hoesft et al. 2006; Nagamine et al. 2006; Scannapieco et al. 2006; Tasker & Bryan 2006; Davé & Oppenheimer 2007; Finlator et al. 2007; Governato et al. 2007; Kobayashi et al. 2007; Tornatore et al. 2007; Finlator & Davé 2008). Most of these works included the treatments of radiative cooling by H & He, star formation, and SN feedback. However, some of the simulations did not include the effects of metal cooling and/or chemical enrichment by galactic wind. Furthermore, the effects of metal cooling on galaxy growth and cosmic SF history has not been explored in detail using cosmological hydrodynamic simulations and presented in the literature, as it is costly to run large cosmological simulations with and without the effect of metal cooling.

In this paper, we investigate the effects of metal cooling and metal enrichment on galaxy growth and cosmic SF history using a series of cosmological hydrodynamic simulations with and without metal cooling. The aim of this paper is to single out the effects of metal cooling among our simulations. This work can be regarded as our initial step towards the long-term goal of developing more complete cosmological hydrodynamic code with physically motivated models of star formation and feedback.

The paper is organised as follows. In § 2, we describe our simulation method focusing on how we implement the metal cooling. In § 3, we study the metal cooling effects on the global properties, such as cosmic SFR, phase space (ρ vs. T) distribution of gas, and the evolution of four phases (hot, warm-hot, diffuse, and condensed) of baryons. We then study the galaxy mass functions (§ 4) and gas mass fractions (§ 5). Finally, we discuss and summarise our findings in § 6.

2 NUMERICAL TECHNIQUE

2.1 Simulation and Metal Cooling

We use the updated version of the Tree-particle-mesh (TreePM) smoothed particle hydrodynamics (SPH) code GADGET-2 (Springel 2005) for our cosmological simulations. The gravitational dynamics is computed by a TreePM algorithm, which uses a particle-mesh method (Hockney & Eastwood 1988) for the long-range gravitational force and a Tree method for the short-range gravitational force (Barnes & Hut 1986). This hybrid algorithm makes the gravitational force calculation faster than a Tree method and allows better force resolution than a PM method in dense regions. The gas dynamics is computed by

an SPH method. The SPH is particularly useful if the simulation needs to resolve large dynamical range, which is an inevitable requirement for the study of galaxy formation in a cosmological context. Therefore a TreePM-SPH simulation can provide a fast and high resolution calculation for both gravitational dynamics and hydrodynamics.

The GADGET-2 code adopts the entropy-conservative formulation (Springel & Hernquist 2002), which alleviates the overcooling problem that previous SPH codes suffered from. Our basic simulations include radiative cooling and heating processes for hydrogen and helium using a method similar to Katz, Weinberg & Hernquist (1996). An external UV background radiation is treated as a spatially uniform photoionising radiation (Haardt & Madau 1996), and modified to match the Ly α forest observations (Davé et al. 1999). Implementing star formation and feedback from first principles is not feasible in current cosmological simulations, because the spatial & mass-scales of molecular clouds are not resolved. Star formation and SN feedback are represented by the subgrid multiphase ISM model developed by Springel & Hernquist (2003a). In the multiphase scheme, a single gas particle represents both hot and cold gas. The stars are formed in the cold portion when the density exceeds a given threshold, ρ_{th} , which is derived self-consistently within the multiphase ISM model. The related parameters, such as the normalisation of gas consumption time and evaporation efficiency of cold gas, are set to satisfy the empirical Kennicutt-Schmidt law (Kennicutt 1998a,b). The SN feedback returns some fraction of the cold gas to the hot phase, and increases the thermal energy of the hot gas.

As an extension to the multiphase ISM model, the simulation includes a phenomenological model for SN-driven galactic wind (Springel & Hernquist 2003a). The galactic wind is particularly important for distributing the metals produced by SNe into the IGM. We use the strong kinematic wind with a velocity of 484 km s^{-1} . It has been shown that this model produces favourable results for the luminosity function of Lyman-break galaxies at the bright-end (Nagamine et al. 2004) and the H I column density distribution function (Nagamine, Springel & Hernquist 2004) at $z = 3$, when compared to the runs without the wind.

However, Davé & Oppenheimer (2007) pointed out the problems of this galactic wind model by comparing with the observations of C IV absorption lines in quasar spectra, and suggested that the momentum-driven wind model (Murray et al. 2005) is a more viable model, which can carry more metals with lower wind velocities. In this paper we choose not to modify our galactic wind model in order to single out the effects of metal cooling, and to allow direct comparisons to the previous works (Nagamine et al. 2004, 2005a,b). Here we focus on the effects of metal cooling on galaxy growth, while Davé & Oppenheimer (2007) focused on the C IV statistics of the IGM.

The metallicity of gas particles are also tracked by the code, assuming a closed box model for each gas particle. The yield ($y = \Delta M_{\text{metal}} / \Delta M_{\text{gas}}$) of 0.02 is assumed. In principle, there could be a time delay between SN explosions and chemical enrichment of the ambient gas. Unfortunately, current cosmological simulations do not have sufficient resolution to track the detailed mixing process of metals. In our simulations, we ignore this time delay and assume an instantaneous mixing within each gas particle. This assumption is

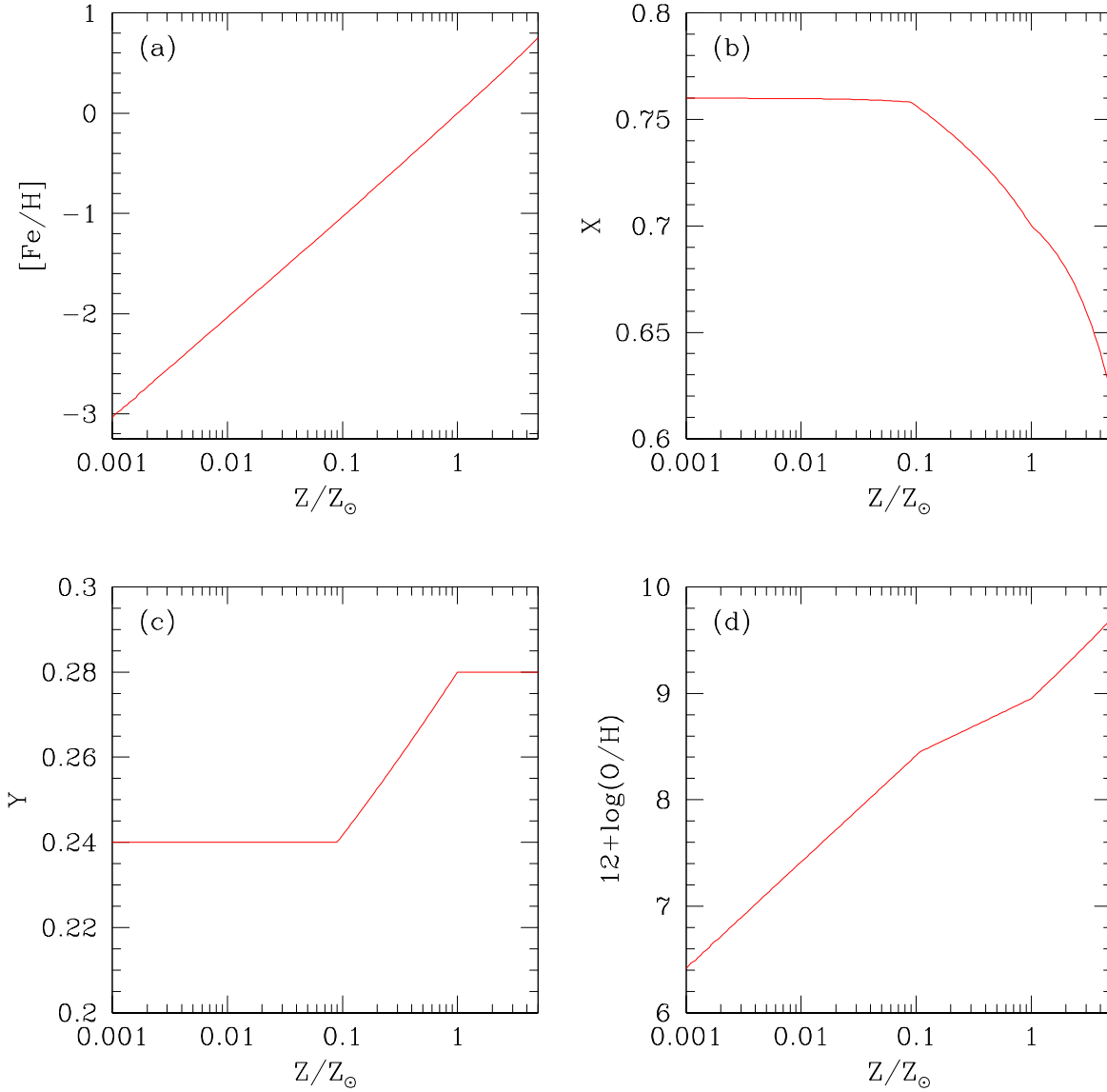


Figure 1. The relationship between metallicity parameters in our implementation of metal cooling. The four panels show the following quantities as a function of metallicity Z/Z_{\odot} , where Z_{\odot} is the solar metallicity. $[\text{Fe}/\text{H}]$, hydrogen mass fraction X , helium mass fraction Y , and oxygen abundance $12 + \log(\text{O}/\text{H})$. Panel (d) represents how α -particles contribute to the metal evolution.

reasonable, because the overall time step of the simulations is longer than the mixing time-scale on small scales.

Ideally we would like to track individual metals and compute the cooling rate of each element at each time-step of the simulation. This approach has been used to study the evolution of individual galaxies (Recchi et al. 2001; Lia et al. 2002; Kawata & Gibson 2003; Kobayashi 2004). For cosmological simulations, it requires a large memory to track individual metals and the computation becomes exceedingly expensive (but see Scannapieco et al. 2005; Martínez-Serrano et al. 2008, for such an attempts). Our simulations collectively track the total mass fraction of metals ($Z \equiv m_{\text{metal}}/m_{\text{gas}}$) as the measure of metallic-

ity. We obtain the chemical abundance and cooling rates for a given Z and temperature by interpolating the table given in Sutherland & Dopita (1993, hereafter SD93) for the standard collisional ionisation equilibrium model, and create a lookup table. Metal cooling is implemented in the full range of metallicity in the table from SD93, from $[\text{Fe}/\text{H}] = -3$ to $[\text{Fe}/\text{H}] = 1$. In addition, the metal cooling outside of this range is computed by extrapolating the table. We require that the extrapolation does not go lower than the primordial cooling rate. The primordial abundance pattern is used where $[\text{Fe}/\text{H}] \leq -1$ (Wheeler et al. 1989; Bessell et al. 1991), and the solar abundance pattern is used where $[\text{Fe}/\text{H}] \geq 0$ (Anders & Grevesse 1989). For $-1 < [\text{Fe}/\text{H}] < 0$, the

abundance pattern is computed by interpolating between the primordial and solar abundance patterns. Note that, $[\text{Fe}/\text{H}] = \log(n_{\text{Fe}}/n_{\text{H}}) - \log(n_{\text{Fe}}/n_{\text{H}})_{\odot}$, where n is the number density.

Figure 1 shows the relationships between the metal parameters ($[\text{Fe}/\text{H}]$, X , Y , and $12 + \log(O/H)$) and the total metallicity Z . Because the abundance pattern is fixed for a given Z , $[\text{Fe}/\text{H}]$ is a monotonically increasing function of Z . The main difference between the solar and the primordial abundance pattern is the oxygen or α -particle enhancement. In the early phase of metal enrichment, Type II SNe are the main source of metals and they tend to generate more α -particles than SN Ia. Therefore, it is expected that a low metallicity gas to have more α -particles than the high metallicity one. As mentioned above, we use two different chemical abundance pattern (at low- and high-end of the Z values) to model this evolution in chemical composition. We compute the oxygen abundance based on the Table 4 of SD93. In our code, we incorporate the metal cooling effect by adding the additional cooling contribution from metals on top of the primordial cooling rate, which is computed in a similar fashion as described in Katz et al. (1996).

Metal enrichment changes the mean molecular weight μ , which is needed to compute the temperature and internal energy of gas. In order to compute μ , we need to know the electron number density n_e , which varies with metallicity. We obtain the values of n_e from SD93 in the same way as we obtained the metal cooling rates. Our electron number density estimate ignores the electrons from photoionised metals by the UV background radiation, but we expect that the number of electrons from ionised metals will be small.

Varying the mean molecular weight μ also influences the SF threshold density ρ_{th} in the multiphase ISM model of Springel & Hernquist (2003a), as well as the cold and hot gas fractions of multiphase gas particles. In this paper, we consider two different treatments of ρ_{th} . In the ‘constant ρ_{th} ’ model, we take the value of ρ_{th} as in the original formulation by Springel & Hernquist (2003a) and do not modulate ρ_{th} by the varying μ . In the ‘varying ρ_{th} ’ model, we take into account of the modulation of ρ_{th} by the change in μ .

2.2 Simulation Setup

We use three series of simulations with varying box size and resolution. The effects of metal enrichment and metal cooling are tested by comparing the runs listed in Table 1. The effects of galactic wind are also tested by turning on and off the wind. The adopted cosmological parameters of all simulations are $(\Omega_m, \Omega_\Lambda, \Omega_b, \sigma_8, h) = (0.3, 0.7, 0.04, 0.85, 0.7)$, which mostly concur with the results of the Wilkinson Microwave Anisotropy Probe (WMAP1) (Spergel et al. 2003).

Our naming conventions for the simulations are as follows. The first part of the run name denotes the particle number and box size used for the simulation series. The run with the extension of ‘mc’ (for ‘metal cooling’) adopts the ‘constant ρ_{th} ’ model for metal cooling, the run with the extension ‘mv’ (for ‘metal, varying’) adopts the ‘varying ρ_{th} ’ model, the run with the extension ‘nw’ has no galactic wind, and the run without any extension uses the cooling rates for the primordial chemical composition (i.e., only H and He).

The ‘N216L10’ series is the fiducial simulation set in our

study. We implement one simulation without galactic wind (‘N216L10nw’ run). The ‘N216L10’ run has the same physical models as the ‘Q4’ run used in Springel & Hernquist (2003b) and Nagamine et al. (2004) with no metal cooling.

To examine the resolution effect, we implement lower resolution simulations, the ‘N144L10’ series. Owing to the comparably small box size and missing long wavelength perturbations, we evolve the N144L10 and N216L10 series only down to $z = 2.75$. To evolve the simulation toward lower redshifts, we need a simulation with a larger box size. Therefore we implement the ‘N288L34’ series, which has a larger box size than other series, but a lower resolution. This series is evolved down to $z = 1$. The runs within the same series use the identical initial condition, which makes the comparison more robust and enables halo-by-halo comparison if needed.

2.3 Galaxy finding method

In cosmological simulations, dark matter, gas, and stars are represented by particles, and these particles are Monte Carlo representations of matter distribution. In order to study galaxy formation using a cosmological simulation, we need a working definition for simulated galaxies. In this paper the simulated galaxies are defined as isolated groups of star and gas particles, identified by a simplified variant of the SUBFIND algorithm developed by Springel et al. (2001). In more detail, the code first computes a smoothed baryonic density field to identify candidate galaxies with high density peaks. The full extent of these groups are found by adding gas and star particles to the groups in the order of declining density. If all N_{min} ¹ nearest neighbour particles have lower densities, this group of particles is considered as a new group. If there is a denser neighbour, the particle is attached to the group to which its nearest denser neighbour already belongs to. If two nearest neighbours belong to different groups and one of them has less than N_{min} particles, these the two groups are merged. If two nearest neighbours belong to different groups and both of them has more than N_{min} particles, the particles are attached to the larger group, leaving the other group intact. In addition, the gas particles in groups should be denser than $0.01\rho_{\text{th}}$. In this paper we are not concerned with groups without star particles. The fraction of such groups are very small, therefore they do not affect our conclusions.

3 GLOBAL PROPERTIES

3.1 Cosmic star formation history

Figure 2 shows the effect of metal cooling and galactic wind on the cosmic SF history for the N216L10 series. The comparison of N216L10mc and N216L10 runs clearly shows that metal cooling enhances the cosmic SFR throughout all redshifts by 20 – 30%. Previously, Hernquist & Springel (2003, Fig. 13) argued that the SFR density is enhanced by metal cooling mostly at lower redshifts and hardly at high- z , however, our simulations suggest otherwise. (See § 6 for more discussion on this point.)

¹ N_{min} is the minimum number of gas and star particles that constitute one isolated group. In this paper we set $N_{\text{min}} = 32$.

Run	Box size ^a	N_p ^b	m_{DM} ^c	m_{gas} ^d	ϵ ^e	z_{end}	Metal cooling ^f	Wind ^g
N144L10	10.00	2×144^3	2.42×10^7	3.72×10^6	2.78	2.75	No (primordial)	Yes
N144L10mc	10.00	2×144^3	2.42×10^7	3.72×10^6	2.78	2.75	Yes (const. ρ_{th})	Yes
N216L10	10.00	2×216^3	7.16×10^6	1.10×10^6	1.85	2.75	No (primordial)	Yes
N216L10nw	10.00	2×216^3	7.16×10^6	1.10×10^6	1.85	2.75	No (primordial)	No
N216L10mc	10.00	2×216^3	7.16×10^6	1.10×10^6	1.85	2.75	Yes (const. ρ_{th})	Yes
N216L10mv	10.00	2×216^3	7.16×10^6	1.10×10^6	1.85	2.75	Yes (varying ρ_{th})	Yes
N288L34	33.75	2×288^3	1.16×10^8	1.79×10^7	4.69	1.00	No (primordial)	Yes
N288L34mc	33.75	2×288^3	1.16×10^8	1.79×10^7	4.69	1.00	Yes (const. ρ_{th})	Yes

Table 1. The simulations employed in this paper

^a Box size in units of h^{-1} Mpc.

^b Initial particle number of dark matter and gas particles.

^c Dark matter particle mass in units of $h^{-1}M_{\odot}$.

^d Initial gas particle mass in units of $h^{-1}M_{\odot}$. The star particle mass is set to $0.5m_{\text{gas}}$ in our simulations.

^e Comoving gravitational softening length in units of h^{-1} kpc. This is a proxy for the spatial resolution of the simulation, and the N216L10 series has a spatial resolution of physical $\approx 0.5 h^{-1}$ kpc at $z = 3$.

^f ‘Primordial’ means the cooling rate with primordial chemical composition. See § 2.1 for the description of ‘constant ρ_{th} ’ and ‘varying ρ_{th} ’ models.

^g If employed, the wind is a ‘strong’ wind with $v_w = 484 \text{ km s}^{-1}$.

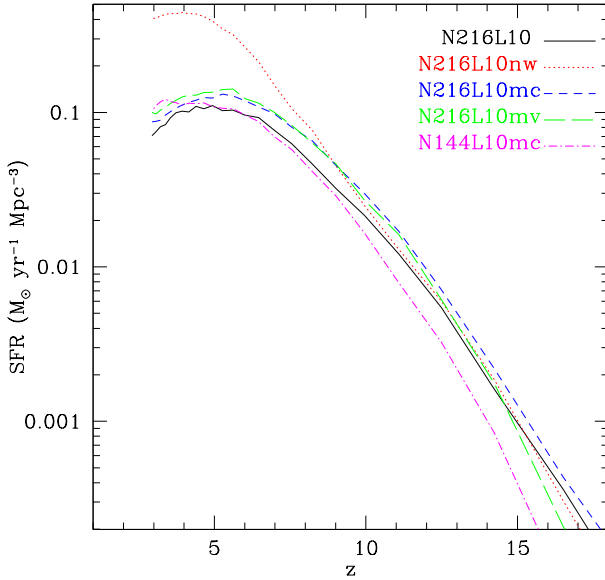


Figure 2. Cosmic star formation histories for the N216L10 series, comparing the runs with and without metal cooling. It also shows the run without a galactic wind (N216L10nw), and a lower resolution run (N144L10mc). Overall the SFR density is increased by $\sim 20 - 30\%$ by metal cooling throughout the entire redshift range.

Metallicity needs to be higher than $\sim 10^{-2}Z_{\odot}$ to noticeably increase the gas cooling rate, because the metal cooling rate is much smaller than that by H and He at $Z \leq 10^{-2}Z_{\odot}$. The metallicity of diffuse IGM is generally lower than $10^{-2}Z_{\odot}$ at $z \gtrsim 3$, and the metal cooling effect on IGM is small. However the local SFR could be enhanced significantly even at high- z when the ISM is enriched to $Z > 10^{-2}Z_{\odot}$, which can be easily achieved after a few events of SN II. Our results suggest that star formation at high- z

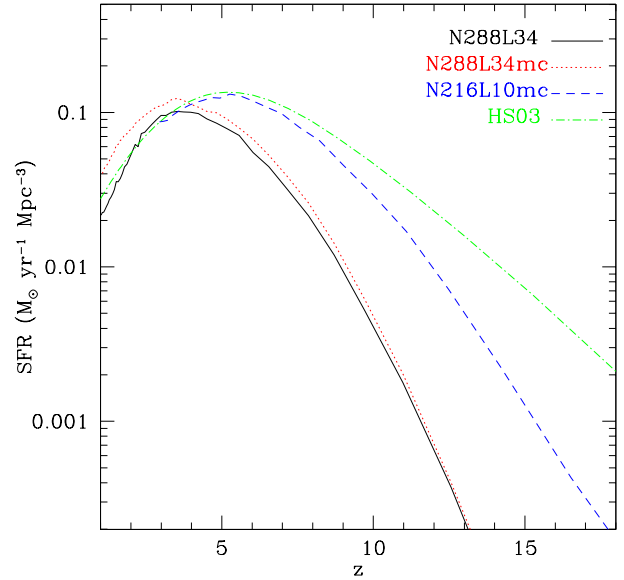


Figure 3. The same as Figure 2, but for the N288L34 series, which goes down to $z = 1$. The N216L10mc run is also shown for a resolution comparison. The green dot-dashed line (HS03) is for the analytic model of Hernquist & Springel (2003, Eq. (2)).

can also be enhanced by metal cooling, and not just at low- z . We also find that the peak of the cosmic SF history hardly shifts by the introduction of metal cooling, consistently with the estimate by Hernquist & Springel (2003).

The N216L10mv run has a lower SFR at $z \gtrsim 9$ and a higher SFR at $z \lesssim 7$ than the N216L10mc run. This is because at high- z , the value of ρ_{th} is higher in the ‘mv’ run than in the ‘mc’ run due to lower metallicity and mean molecular weight, leading to a larger fraction of gas not being

able to satisfy the SF criteria in the N216L10mv run than in the N216L10mc. The opposite is true at $z \lesssim 3$.

Figure 2 also shows that the SFR in the N216L10nw run is higher than other runs by an order of magnitude. This is because the gas can cool very efficiently without being ejected by the galactic wind. Although the current galactic wind models in cosmological simulations are not well established yet and need to be improved, both theoretical and observational studies evidently suggest the important role of galactic wind feedback (Springel & Hernquist 2003a; Martin 2005, 2006; Oppenheimer & Davé 2006).

As expected, the N144L10mc run has lower SFR densities at $z \geq 7$ compared to the N216L10 series. This is because a lower resolution run is unable to resolve low-mass halos that would otherwise form stars in them. When the star formation at high- z is underestimated, some of the gas remain unconverted into stars until lower redshift, resulting in a higher SFR at $z < 4$ in the N144L10mc run than in the N216L10mc run.

Figure 3 shows the cosmic SF history down to $z = 1$ for the N288L34 series. Again, the SFR density in the N288L34mc run is systematically higher than that in the N288L34 run at all redshifts. Moreover, the difference in SFR density between the two runs increases at $z \lesssim 3$. By $z \sim 3$ the IGM metallicity becomes high enough to noticeably increase the cooling rate, and the accretion of IGM onto galaxies becomes more efficient, which later fuels the star formation. Our results suggest that the cosmic SFR density is enhanced by metal cooling at $z \lesssim 3$ by both of the following two effects: 1) more efficient IGM accretion onto galaxies due to higher metallicity of IGM, and 2) increased SF efficiency due to higher cooling rate with the contribution from metal cooling.

In Figure 3 the analytic model of Hernquist & Springel (2003, Eq. (2), hereafter H&S model) is also shown in the green dot-dashed line. This model is a result of many cosmological SPH simulations with increasing resolution, and the authors gave a theoretical interpretation to the empirical fitting formula for the cosmic SFR density. Since our runs adopt a lower value of $\sigma_8 = 0.85$ than the original value used to derive the H&S model ($\sigma_8 = 0.90$), we modify the H&S model by rescaling the β parameter in their Eq. (2) and Eq. (47). This reduces the SFR density at $z \gtrsim 5$ by $\sim 10\%$, but not much at $z \lesssim 5$. The results of the N288L34 and N216L10mc runs agree well with the H&S model at $z < 4$ and $z < 6$, respectively. This is expected, because the N288L34 run adopts the same physical models as in the original simulations that were used to derive the H&S model. At high- z , both runs fall short compared to the H&S model owing to insufficient resolution.

3.2 Phase space distribution of cosmic gas

The metal enrichment and metal cooling also change the phase space distribution ($\rho-T$ diagram) of cosmic gas. Figure 4 shows the state of cosmic gas at $z = 3$ for the N216L10 series. As shown in panel (a), the baryons in the Universe can be broadly categorised into four different phases according to their overdensity and temperature: ‘hot’, ‘warm-hot’, ‘diffuse’, and ‘condensed’ (Davé et al. 1999; Cen & Ostriker 1999; Davé et al. 2001). The first two phases are mostly the shock-heated gas in clusters and groups of galaxies.

The ‘diffuse’ phase is mostly the photoionised IGM with lower temperature, which can be observed as the Ly α forest. The tight power-law relationship between ρ and T at $\rho/\bar{\rho} \lesssim 3$ and $T < 10^4$ K is governed by the ionisation equilibrium (Hui & Gnedin 1997), where $\bar{\rho}$ is the mean density of baryons at $z = 0$.

The ‘condensed’ phase is the high density, cold gas in galaxies. Because the primordial cooling curve has a sharp cutoff at $T \simeq 10^4$ K, the temperature of condensed phase decreases only down to this temperature in Figure 4a,b. The characteristic finger-like feature at $\rho/\bar{\rho} \gtrsim 10^4$ is due to the pressurisation of the star-forming gas by SN feedback in the multiphase ISM model of Springel & Hernquist (2003a). A fitting formula for this effective equation of state was derived by Robertson et al. (2004), which is shown by the blue dashed lines. Above the SF threshold density ρ_{th} , the gas particles in the simulation go into the multiphase mode and are allowed to form stars.

The most noticeable and interesting change in the $\rho-T$ plot by the metal cooling is in the distribution of ‘condensed’ gas. Star formation and SN explosions occur in the multiphase star-forming gas, therefore the immediate effect of metal cooling appears in the condensed phase. The presence of gas at $T < 10^4$ K with metal cooling results from the effective temperature calculation for the multiphase medium, and not from the direct gas cooling down to $T < 10^4$ K. According to the multiphase scheme in Springel & Hernquist (2003a), the star forming gas consists of two phases: hot gas (10^5 K $< T < 10^8$ K) and cold gas ($T = 10^3$ K). The effective temperature for the multiphase gas is computed from the internal energy of hot and cold gases, which are derived using the cold gas fraction. The cold gas fraction is computed from the cooling rate of hot gas and the gas density. The original GADGET imposes the effective temperature of 10^4 K at the SF threshold density. In our metal cooling scheme, however, the cooling rate of hot gas increases, and the cold gas fraction increases. Therefore, the multiphase gas above the SF threshold density with higher metallicity could have lower effective temperature of $T < 10^4$ K in our implementation.

In the N216L10mc run, the value of ρ_{th} was kept fixed as the original value, which causes a sharp edge at $\rho/\bar{\rho} \simeq 10^4$ for the multiphase gas. In the N216L10mv run, the value of ρ_{th} was varied according to the change in mean molecular weight, therefore the condensed gas has a spread in both temperature and density near $\rho/\bar{\rho} \simeq 10^4$.

Galactic wind returns the metal-enriched, star-forming gas to the hot and low density IGM, as evidenced in the $\rho-Z$ diagrams. This metal-enriched, low-density ($\rho/\bar{\rho} \lesssim 10$) gas is absent in the N216L10nw run, which clearly shows the necessity of galactic wind to explain the metallicity observed in Ly α forest. The phase distribution of IGM in the N216L10, N216L10mc, and N216L10mv runs are very similar. This is presumably because the effects of metal cooling is not so significant yet in the IGM at $z > 3$. As we will discuss in the next section, this is not the case at $z < 3$.

3.3 Evolution of four phases of baryons

The connection between the four phases of cosmic gas is important in galaxy formation, and it is beneficial for us to study their evolution for a better understanding of metal cooling effects. A conventional view is that the dif-

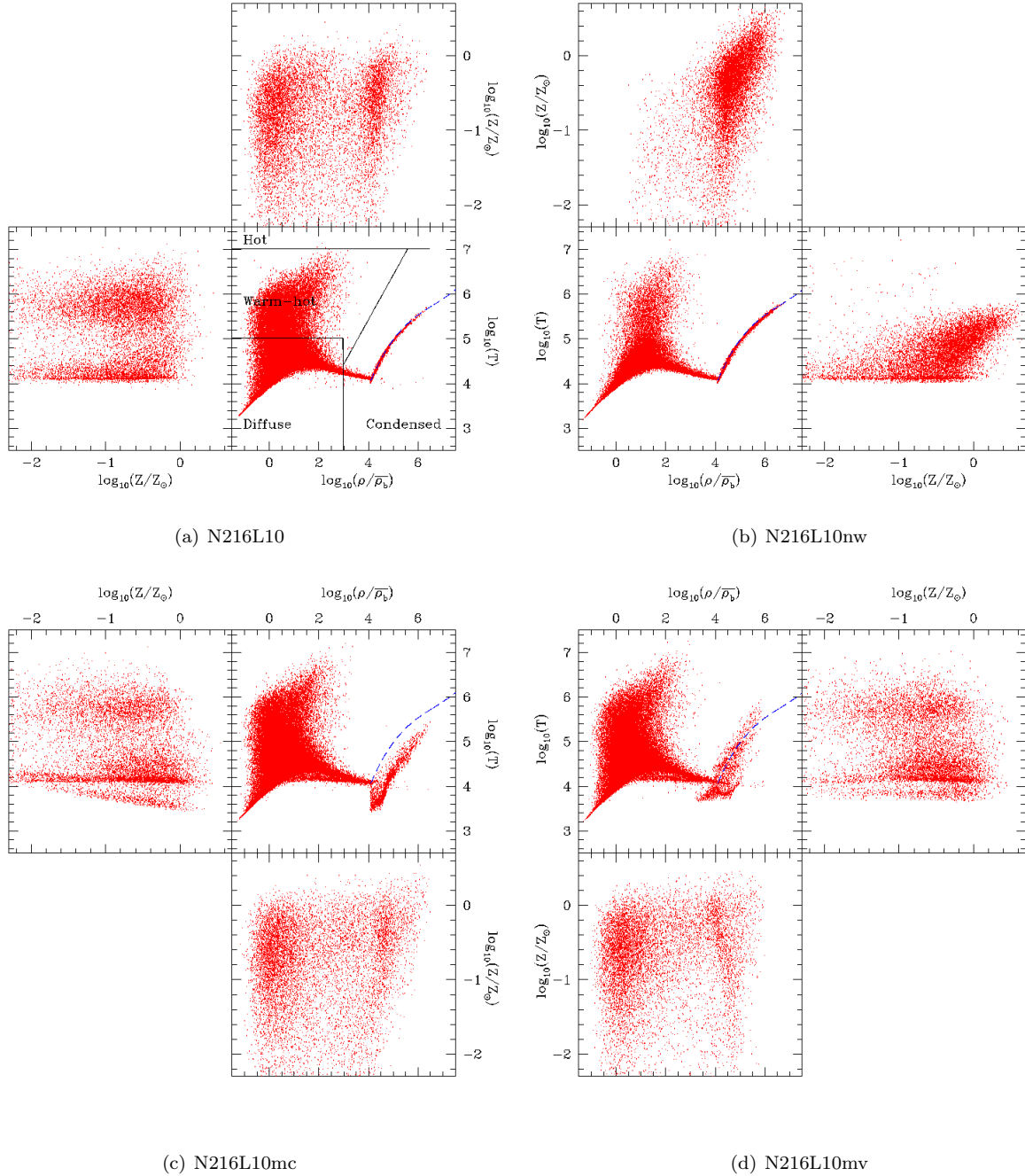


Figure 4. The phase space and metallicity distribution of the cosmic gas at $z = 3$ for the four simulations of N216L10 series. For each run, three panels are shown for $\rho - T$, $Z - T$, and $\rho - Z$ relationship. For plotting purpose, we plot only randomly selected 1% of the total gas particles in the simulation. The blue dashed line is based on the fitting function to the effective equation of state for the multiphase star-forming gas provided by Robertson et al. (2004).

fuse gas is shock-heated to hot or warm-hot phase, which later cools down to the condensed phase (Davé et al. 1999; Cen & Ostriker 1999; Davé et al. 2001). Kereš et al. (2005) also suggested that some diffuse gas can migrate to the condensed phase without being shock-heated, which they called the ‘cold mode’ accretion.

Figure 5 shows the evolution of mass fractions of different phases. All of our simulations show that the diffuse

phase continuously decreases from high- z to low- z , while the ‘warm-hot + hot’ and ‘condensed’ phases continuously increase, consistently with the general expectations. The IGM (i.e., hot + warm-hot + diffuse) is accreted onto galaxies, to become the condensed phase. The diffuse component (panel a) decreases from $\approx 95\%$ at $z = 6$ to $\approx 55\%$ at $z = 1$. The ‘warm-hot + hot’ component (panel b) increases from almost zero at $z = 6$ to $\approx 35\%$ at $z = 1$. The mass fraction

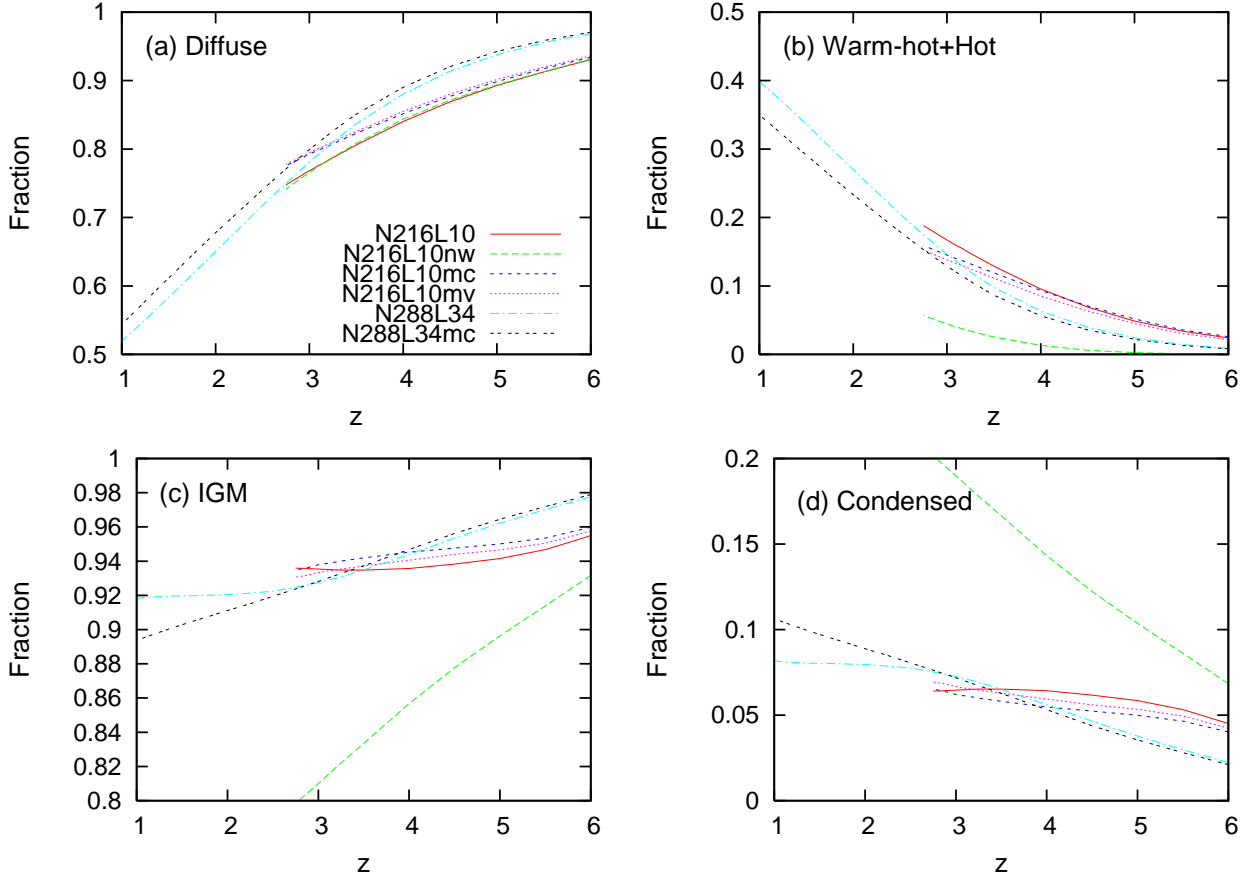


Figure 5. The evolution of mass fractions for the four phases of baryons: hot, warm-hot, diffuse, and condensed. *Panel (b)* shows the addition of the two phases, ‘warm-hot + hot’, and *panel (c)* shows the total masses in the IGM, i.e., ‘diffuse + warm-hot + hot’. Here we compare the N216L10 and N288L34 series.

of the total IGM (panel *c*) decreases from 96 – 98% at $z = 6$ to 92 – 93% at $z = 3$. This reflects the increase of the condensed phase (panel *d*) from a few percent at $z = 6$ to $\sim 7\%$ at $z = 3$. These mass fractions are in general agreement with the results of Davé et al. (2001).

The comparison between N288L34 and N288L34mc runs shows interesting differences. At $z > 3$, the mass fractions of all four phases are similar in the two runs. However, at $z < 3$, the IGM mass fraction continues to decrease in the N288L10mc run, while it becomes almost constant in the N288L10 run. A similar behaviour is seen for the condensed phase, and the N288L10mc continues to increase its condensed mass. This suggests that the metal cooling enhances the IGM accretion onto galaxies mostly at $z \lesssim 3$, which supplies the fuel for star formation. The cooling of warm+hot phase into diffuse phase is also enhanced, leading to a larger mass fraction of diffuse component in the N288L34mc run than in the N288L34 run. (The same is true for N216L10mc and N216L10 runs.)

The N216L10nw run shows stark differences from all other runs. It has a significantly lower IGM mass fraction, and a very large mass fraction in the condensed phase. This shows that the IGM is mostly enriched by galactic wind, and that most of the masses are returned into the ‘warm-hot + hot’ phase, but not to the diffuse phase.

4 GALAXY STELLAR & BARYONIC MASS FUNCTION

4.1 At $z \geq 3$:

Galaxy stellar mass function (GSMF) tells us how the stellar mass is distributed in different galaxies, and its redshift evolution reflects the growth of structure in the hierarchical universe. Figure 6 compares the GSMF in different simulations. We only show the range of $M_{\text{star}} \geq 2.5 \times 10^7 M_{\odot}$, which corresponds to the limiting mass of 32 star particles in N216L10 runs. We chose 32 star particles as our resolution limits because all mass function start to turn over around this mass range. Panel (a) shows that the run with no galactic wind (N216L10nw) completely overestimates the GSMF, and the run with lower resolution (N144L10) underestimates the number of lower mass galaxies at $M_{\text{star}} \lesssim 10^8 M_{\odot}$ relative to the N216L10 run. Panel (b) shows that the metal cooling increases the masses of galaxies by $\sim 20\%$ at $z = 3$. As a result, both the N216L10mc and N216L10mv runs show a slight increase in the number of galaxies at the massive end, with a slightly stronger enhancement in the N216L10mv run.

Figures 6c,d demonstrate that the metal cooling also changes the redshift evolution of GSMF. In the N216L10mc run, the peak of mass function is shifting more toward the massive side than in the N216L10 run at $z = 3$. From $z = 4$ to $z = 3$, the low-mass galaxies merge to form more massive

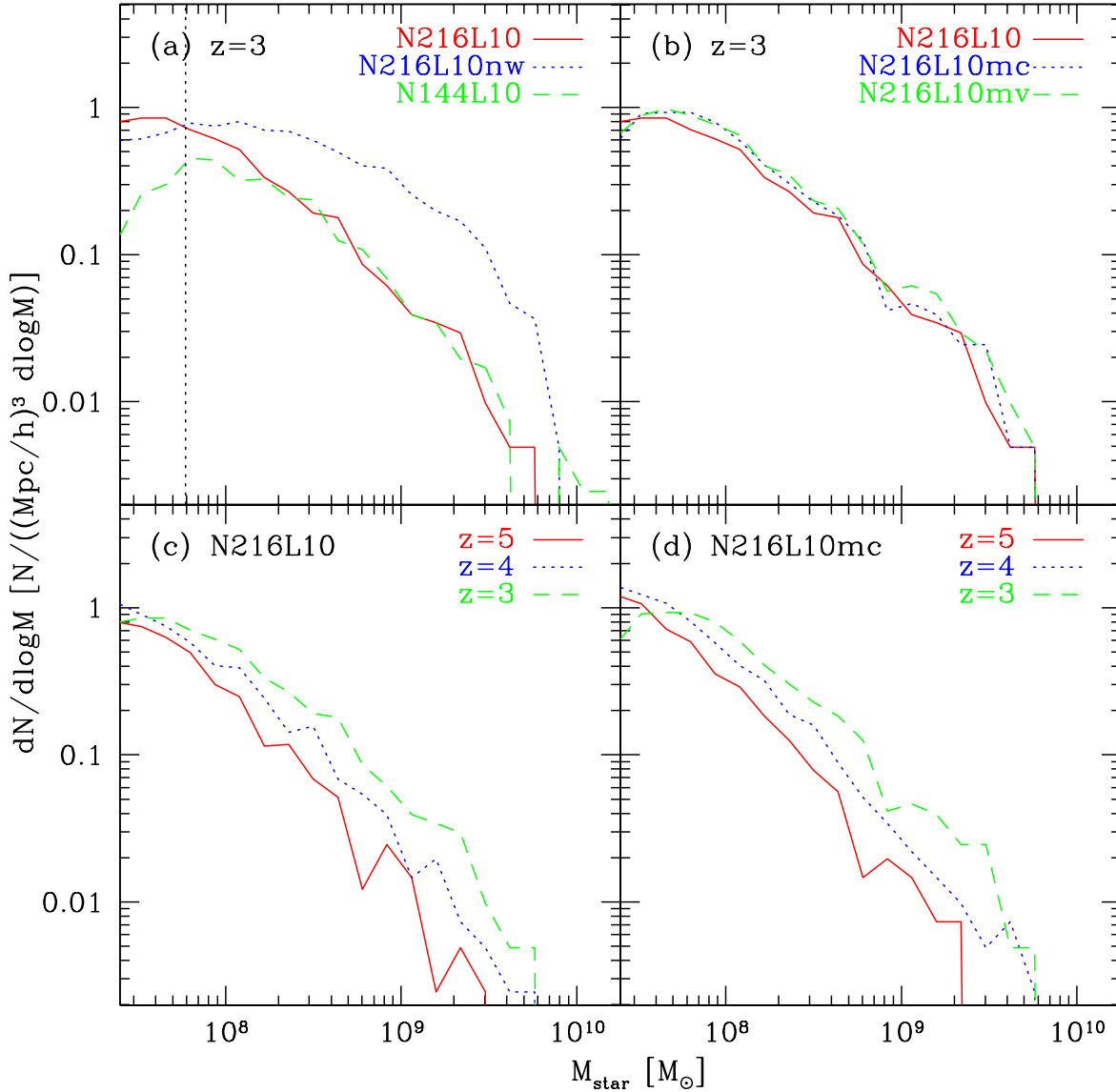


Figure 6. Stellar mass functions of simulated galaxies. *Panel (a):* For the runs without metal cooling at $z = 3$. The vertical dotted line indicates the galaxy masses with 32 star particles for N144L10 run. *Panel (b)* compares the N216L10 series at $z = 3$. The bottom two panels show the redshift evolution of GSMF in the N216L10 (*panel c*) and N216L10mc (*panel d*) run.

galaxies, increasing the number of galaxies with $M_{\text{star}} > 10^8 M_{\odot}$ furthermore.

It also seems that the formation of low-mass galaxies ($M_{\text{star}} \lesssim 10^8 M_{\odot}$) is enhanced by metal cooling at early times ($z = 5-6$). However we find that the behaviour of MF at the low-mass end is somewhat dependent on the threshold density for the grouping. As mentioned in § 2.3, our grouping code imposes a threshold gas density of $0.01\rho_{\text{th}}$ for a gas particle to be part of a galaxy. When we lower this threshold density, we find that the two MFs for the N216L10 and N216L10mc converged, as more particles are incorporated into galaxies at the outskirts of galaxies. Metal cooling increases the gas density in galaxies, enabling more low-mass

galaxies to satisfy the gas density threshold and to be identified as simulated galaxies. Therefore the behaviour of MF at $M_{\text{star}} \lesssim 5 \times 10^7 M_{\odot}$ is somewhat dependent on the choice of the outer threshold density of galaxies.

Figure 7 compares the gas and baryonic (star + gas) MFs for the N216L10 series at $z = 3$ (panels *a* & *b*), and the redshift evolution of the baryonic MF from $z = 5$ to $z = 3$ in the N216L10 (panel *c*) and N216L10mc (panel *d*) runs. Here we show only the range of $M_{\text{star}} \geq 5.0 \times 10^7 M_{\odot}$, which corresponds to the limiting mass of 32 gas particles. Panel (*a*) shows that more gas is converted into stars in the runs with metal cooling (N216L10mc and N216L10mv) compared to the N216L10 run, while panel (*b*) shows that the baryonic

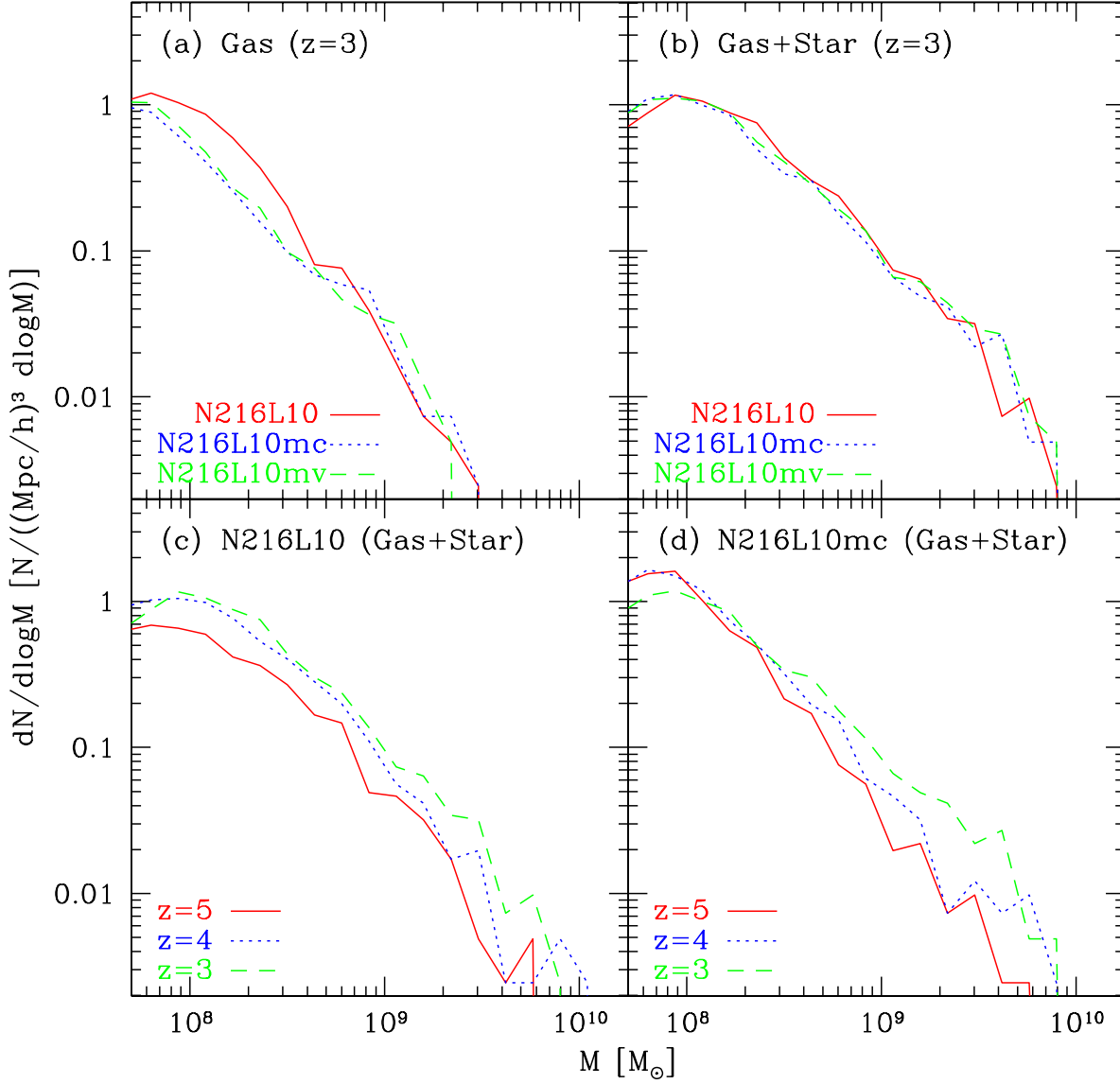


Figure 7. The stellar (*panel a*), gas (*panel b*), and the total baryonic (*panel c*) mass functions for the N216L10 series at $z = 3$.

MF is similar in all the runs. As we discussed in § 3.3, the IGM accretion onto galaxies is not so much enhanced yet before $z \sim 3$ due to relatively low IGM metallicity, which explains the similarity in the total baryonic MF. In the runs with metal cooling, the peak of GSMF is shifted toward higher mass, whereas the peak of gas MF is shifted toward lower mass. This suggests that the enhanced GSMF at $z = 3$ is due to the increased SF efficiency by metal cooling within the galaxies. Again, the apparent enhancement in the number of low-mass galaxies in the N216L10mc run compared to the N216L10 run is somewhat dependent on the threshold density of grouping, therefore it should be interpreted with caution.

4.2 At $z < 3$:

As the accretion of IGM onto galaxies become more efficient at $z < 3$ due to the increased IGM cooling by the metals, we expect that the total baryonic mass of galaxies would be more enhanced at $z = 1$ than at $z = 3$. Figure 8 shows the MFs at $z = 3$ and $z = 1$ in the N288L34 series, and it clearly demonstrates that this expectation is true. Here we show only the range of $M_{\text{gas}} \geq 8.2 \times 10^8 M_{\odot}$, which corresponds to the limiting mass of 32 gas particles. The general trend in the three (star, gas, and total baryon) MFs is similar to that we saw in Figure 7, although the difference at $z = 3$ between the N288L34 and N288L34mc runs is slightly smaller than in the N216L10 series due to poorer resolution. Figure 8f shows most prominently the enhancement of the

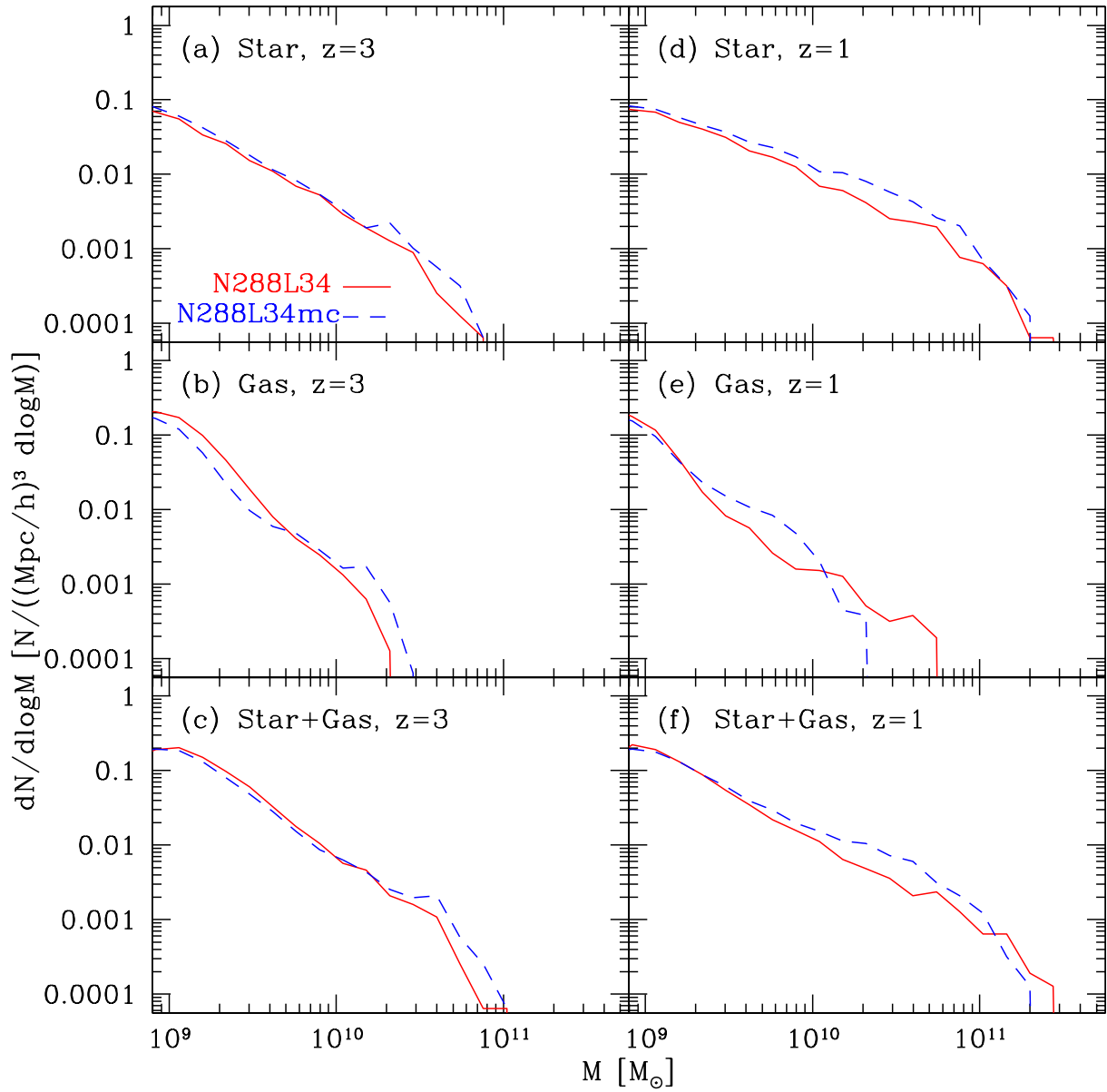


Figure 8. The stellar, gas, and baryonic (star + gas) mass functions at $z = 3$ (left) and $z = 1$ (right) for the N288L34 series.

total baryonic MF at $z = 1$ in the N288L34mc run owing to the metal cooling. In panels (e) & (f), the N288L34 run actually has a longer tail at the most massive-end than the N288L34mc run. The reason for this feature is not fully clear, but it may be related to the balance between IGM accretion and feedback. Owing to metal cooling, IGM accretion rate increases in the 'mc' run, and the SFR is also enhanced, leading to a stronger feedback. The amount of mass loss is greater in low mass galaxies, but the net heating of IGM is more significant for massive galaxies. The 'mc' run has stronger feedback, therefore its feedback heating may become more significant than IGM accretion for very massive galaxies. The significant IGM heating suppresses the growth of massive-end of mass function from $z = 3$ to $z = 1$ and

results in shorter tail for the 'mc' run at $z = 1$ as shown in Figure 8e,f.

5 GAS FRACTION

For a fixed galaxy baryonic mass, the enhancement of star formation by metal cooling would decrease the gas mass fraction, $f_{\text{gas}} \equiv M_{\text{gas}}/M_{\text{baryon}}$. Figure 9 shows f_{gas} as a function of galaxy stellar mass for the N216L10 series. Panel (a) shows the data only from N216L10mc run at $z = 3$, and each data point corresponds to a simulated galaxy. To characterise the distribution, we compute the following two quantities in each logarithmic stellar mass bin: 'average' and 'median'. The 'average' is the ratio of total gas

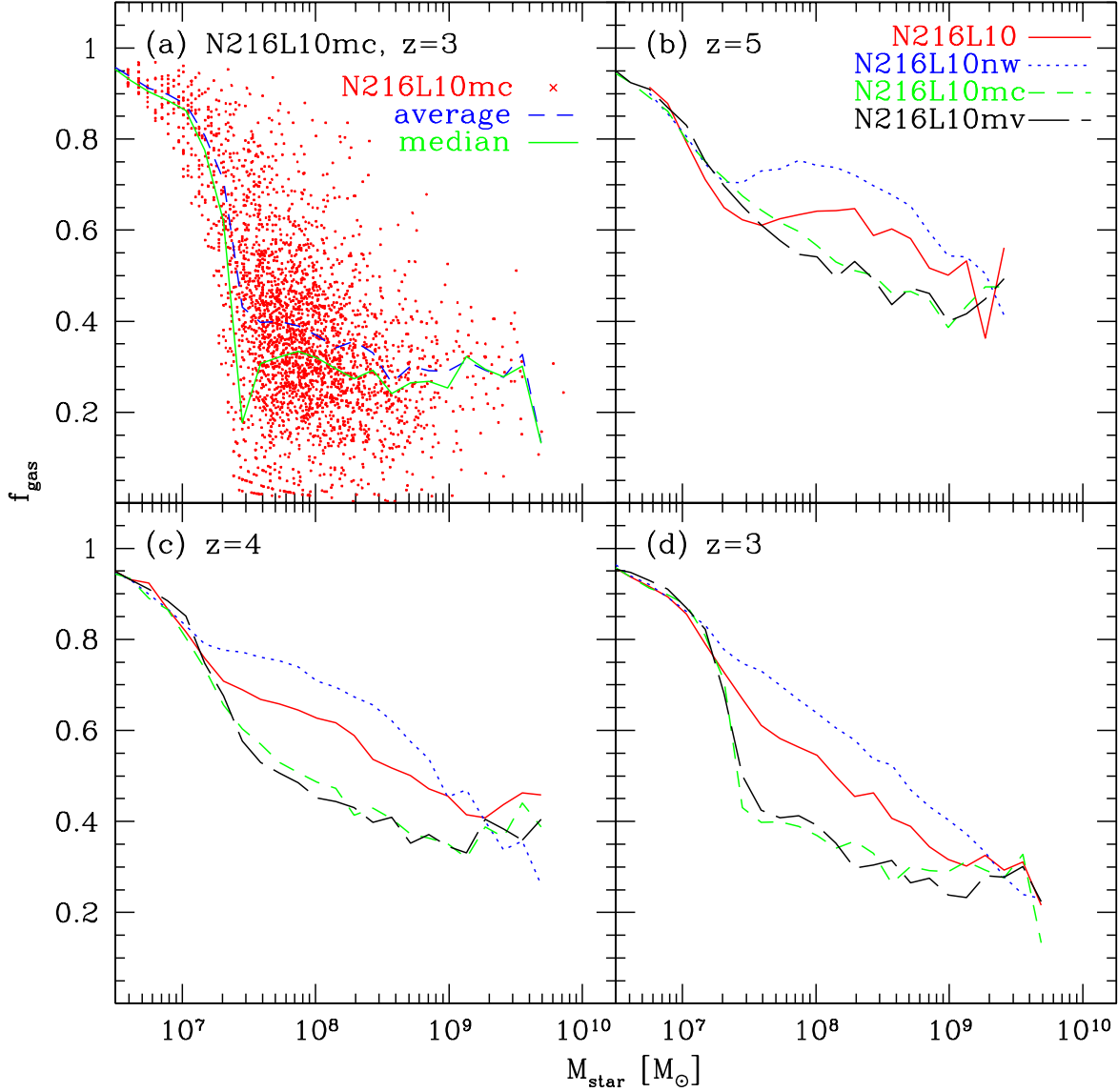


Figure 9. The gas fraction of galaxies as a function of stellar mass. Each data point in *panel (a)* is a simulated galaxy in the N216L10mc run at $z = 3$. Here we overplot two lines representing the distribution: ‘average’ and ‘median’ (see text for details). Panels (b) – (d) compare the gas fractions (‘average’ case) in the N216L10 series at $z = 3, 4$, & 5.

mass to total baryonic mass for all the galaxies in each mass bin, i.e., $\sum_i M_{\text{gas},i} / \sum_i M_{\text{baryon},i}$. The ‘median’ case is simply the median of f_{gas} values in each mass bin. Both quantities show a similar trend, however, there is a sharper drop-off at $M_{\text{star}} \simeq 2.5 \times 10^7 M_{\odot}$ for the ‘median’ case in Figure 9a. This mass-scale corresponds to 32 star particles in the N216L10 series. We find that there are many galaxies with $f_{\text{gas}} = 0$ above this mass-scale, which causes the sharp drop-off in the ‘median’ line. Below this limiting mass, galaxies are not resolved well, which results in an underestimate of star formation and an overestimate of f_{gas} . If we had a higher resolution simulation with finer particle masses, this limiting mass-scale would shift to a

lower mass. Therefore the location of this sharp drop-off is currently determined by the resolution of our simulation. However, dark matter halos would stop forming stars at some lower limiting halo mass, if we had an infinitely high-resolution simulation. This lower limit to the galaxy mass is presumably determined by the photoevaporation of gas by the UV background radiation (Rees 1986; Efstathiou 1992; Quinn et al. 1996; Gnedin 2000; Nagamine et al. 2004; Pontzen et al. 2008; Okamoto et al. 2008). Recent works suggest that star formation could be suppressed by the UV background in halos with $M_{\text{halo}} \lesssim 10^9 M_{\odot}$ at $z \sim 3$. Galaxies with $M_{\text{star}} \simeq 2 \times 10^7 M_{\odot}$ would reside in halos with $M_{\text{halo}} \approx 2 \times 10^9 M_{\odot}$. The N216L10 series would resolve such

a halo with ~ 280 dark matter particles, and its mass resolution is actually close to the astrophysical limit for dwarf galaxy formation at $z \sim 3$. Therefore the sharp drop-off in f_{gas} at $M_{\text{star}} \simeq 2 \times 10^7 M_{\odot}$ may not be so far from the true answer.

We find that f_{gas} increases with decreasing M_{star} at all redshifts, regardless of metal cooling and wind effects. This trend is qualitatively consistent with current observations. Erb et al. (2006) estimate the gas fraction as a function of stellar mass using the rest-frame UV-selected star-forming galaxies at $z \sim 2$, and show that the gas fraction decreases with increasing stellar mass. And using the mean gas and stellar mass, they find the average $f_{\text{gas}} \sim 0.35$, which agrees with the predicted gas fraction for massive galaxies in our simulation. In addition, Geha et al. (2006) reported that the average neutral gas fraction is $\langle f_{\text{gas}} \rangle = 0.6$ for the local dwarf galaxies selected from the Sloan Digital Sky Survey. In our N216L10 series with metal cooling, the ‘average’ f_{gas} reaches 0.6 for galaxies with $M_{\text{star}} \simeq 2 \times 10^7 M_{\odot}$ at $z = 3$ & 4.

Figures 9b,c,d show the redshift evolution of f_{gas} for the N216L10 series. In the runs with metal cooling (N216L10mc and N216L10mv), f_{gas} is lower than in the N216L10 run by 20 – 30% at all redshifts for galaxies with $M_{\text{star}} = 10^{7.5} - 10^9 M_{\odot}$. This result suggests that the metal cooling reduces f_{gas} owing to more efficient star formation. The values of f_{gas} seem to be more convergent at the massive-end ($M_{\text{star}} > 10^9 M_{\odot}$). In addition, we find that galaxies in the N216L10nw run are the most gas-rich, because almost no galactic gas is returned to the IGM.

Figures 9b,c,d also show that f_{gas} is higher at higher redshifts. For example, the well-resolved galaxies with $M_{\text{star}} = 10^9 M_{\odot}$ have $f_{\text{gas}} \simeq 0.45$ at $z = 5$, but $f_{\text{gas}} = 0.25$ at $z = 3$. As we saw in Figure 6d, there is a considerable growth in GSMF from $z = 5$ to $z = 3$. Together with the decrease in the gas fraction, these results suggest that most of the gas accreted during $z = 3 - 5$ has been converted into stars.

Figure 10a highlights the redshift evolution of f_{gas} from $z = 5$ to $z = 1$ in the N288L34mc run. The gas mass fraction clearly decreases with decreasing redshift as the gas is converted into stars. The rate of decrease is greater at $z = 5 \rightarrow 3$ than at $z = 3 \rightarrow 1$, with $f_{\text{gas}} \simeq 0.5, 0.25$, & 0.2 for $z = 5, 3$, & 1 , respectively, for galaxies with $M_{\text{star}} \gtrsim 3 \times 10^9 M_{\odot}$.

Figure 10b shows the effect of resolution on f_{gas} . The location of the drop-off in f_{gas} shifts to lower masses as the resolution is increased from N144L10mc to N216L10mc run. The location of the drop-off is at around our resolution limit – the vertical lines in Panel (b). Therefore the values of f_{gas} are overestimated in unresolved galaxies.

6 DISCUSSIONS AND CONCLUSIONS

Using cosmological hydrodynamic simulations with metal enrichment and metal cooling, we studied their effects on galaxy growth and cosmic SFR. Owing to metal cooling, the SFR density increases about 20% at $z = 3$ and about 50% at $z = 1$. Our results suggest that metal cooling enhances the star formation through two different processes: 1) more efficient conversion of local ISM into stars (i.e., increase of local SF efficiency), and 2) the increase of IGM accretion onto galaxies. The former process is in effect essentially at

all times at $z \lesssim 15$, because the local ISM can be instantaneously enriched by SN explosions. This process enhances the SFR, but does not noticeably change the total baryonic mass of galaxies. The latter process, on the other hand, can increase the total baryonic mass of galaxies, as well as enhancing the overall SFR density by supplying more gas for star formation. This process becomes effective only at lower redshifts ($z \lesssim 3$), because it takes some time to enrich the IGM up to $Z \gtrsim 10^{-2} Z_{\odot}$.

In this paper, we used two different prescriptions for star formation in the runs with metal cooling: 1) the ‘constant ρ_{th} ’ scheme and 2) the ‘varying ρ_{th} ’ scheme. The value of ρ_{th} was fixed in the former scheme, while it was modulated according to the metallicity in the latter scheme. Both schemes show similar increase of cosmic SFR density (see Figure 2), which implies that the overall SF enhancement by metal cooling is not so sensitive to the choice of ρ_{th} (but with some differences as we discussed in § 3.1).

The multiphase ISM model for star formation by Springel & Hernquist (2003a) contains two free parameters: ρ_{th} and the normalisation of gas consumption time-scale, t_{\star}^0 . The values of these two parameters were originally chosen to match the empirical Kennicutt-Schmidt law (Kennicutt 1998a,b) using simulations of isolated disk galaxies. Since we did not change the value of t_{\star}^0 in the runs with metal cooling (as well as ρ_{th} in the ‘mc’ runs), it is possible that our simulations may now violate the Kennicutt law.

However, as we show in Figure 11, the plots of N_{HI} vs. Σ_{SFR} for the N216L10 and N216L10mc runs are not so different from each other. This can be understood as follows. As Figure 5c showed, metal cooling increases the density and lowers the temperature of star-forming gas. The fundamental scaling relationship between SFR and cold gas density does not need to change when the metal cooling is introduced; the star-forming gas particles would simply slide upward along the Kennicutt law, $\Sigma_{\text{SFR}} \propto N_{\text{HI}}^{1.4}$.

In the case of N216L10mv run, we varied ρ_{th} according to the gas metallicity, primarily scattering it to lower values because higher metallicity increases the cooling rate and lowers ρ_{th} . Therefore more gas particles become eligible to form stars and Σ_{SFR} is scattered upward above the Kennicutt law for a given value of N_{HI} , resulting in a broader deviation from the power-law relationship of the Kennicutt law near $\log N_{\text{HI}} \simeq 20$. At higher values of N_{HI} , Σ_{SFR} is enhanced, but still within the range of the Kennicutt law. This difference can be alleviated by adjusting the SF timescale (see Springel & Hernquist 2003a), however, we try to emphasise the effect of metal cooling on SFR by keeping this parameter the same in all the runs. Further investigations of the HI aspect of our simulations is beyond the scope of the present paper, and we will present the results elsewhere.

Upon evaluating the effect of metal cooling, Springel & Hernquist (2003b) considered two different gas phases where the cooling become important. One is the diffuse gas in galactic halos, which must radiate its thermal energy in order to collapse onto the high-density ISM, and the other is the multiphase star-forming gas. They argued in their § 5.2 that the cosmic SFR density at $z \gtrsim 6$ would not be affected by the metal cooling very much, because at high- z cooling is so efficient that the gas in diffuse atmospheres of halos cools nearly instantly, even without any metal cooling. They expected their model results to

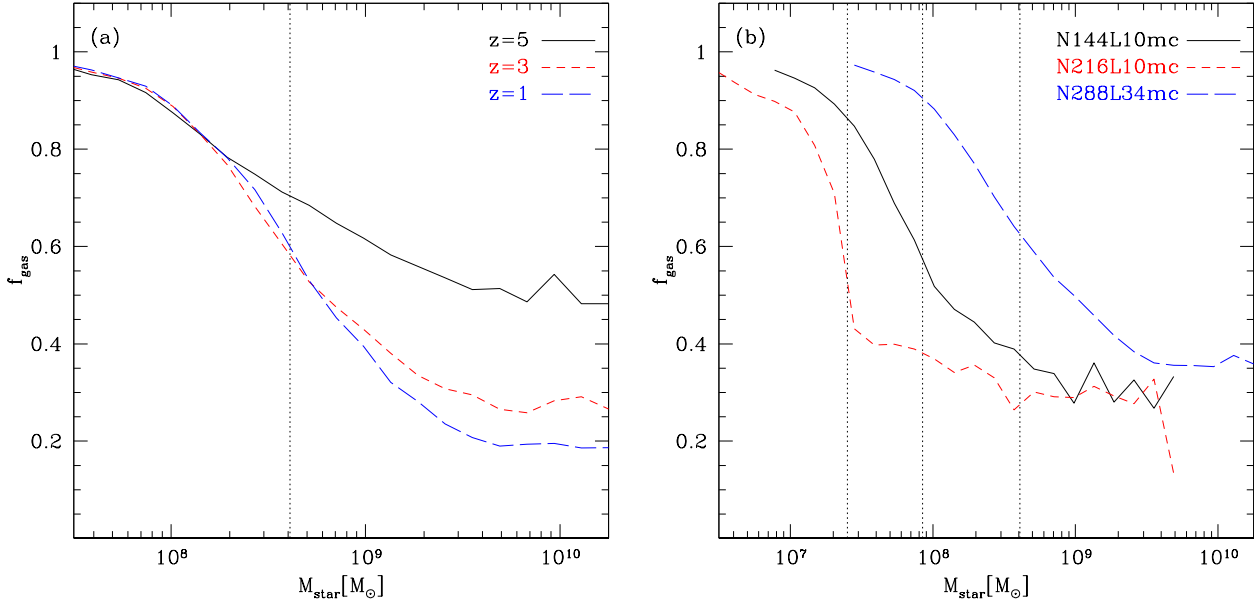


Figure 10. *Panel (a)* highlights the redshift evolution of f_{gas} in the N288L34 run from $z = 5$ to $z = 1$. *Panel (b)* shows the effect of numerical resolution on f_{gas} . The vertical dotted lines indicate the galaxy masses with 32 star particles for each run. The simulation results shift to lower masses as the resolution is increased. We plot the ‘average’ case in these figures.

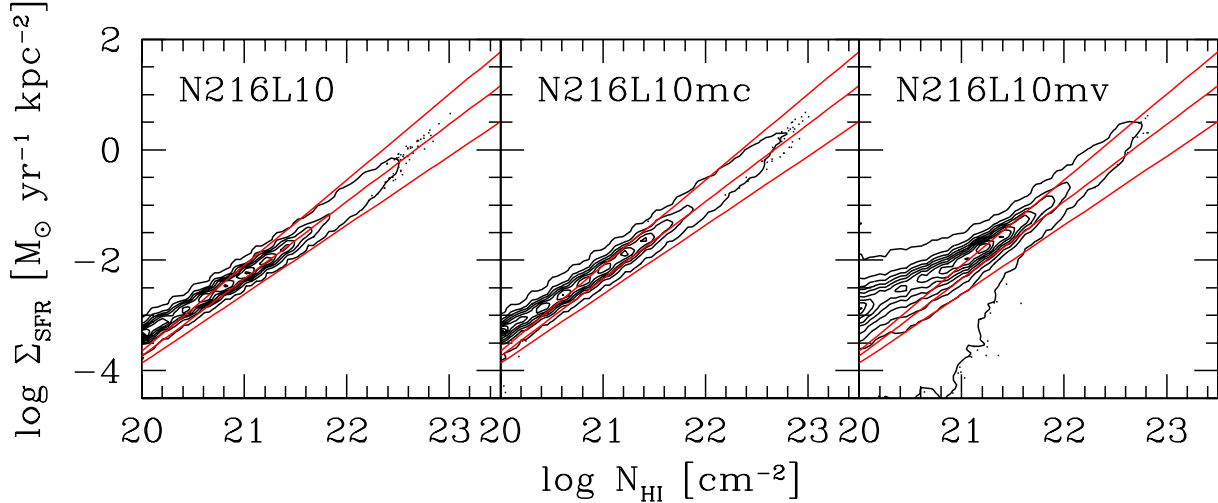


Figure 11. Comparison of the N216L10 series with the empirical Kennicutt law.

be largely independent of metal enrichment, because in this regime the evolution of SFR density is driven by the fast gravitational growth of the halo mass function. For the star-forming multiphase ISM, they argued that the parameters of their model (e.g. cold gas evaporation efficiency and gas consumption time-scale) can be adjusted such that the normalisation of the Kennicutt law can be maintained, yielding to first order unaltered model predictions. However, our simulations, in particular the comparison between the N216L10 and N216L10mc run, suggest that the metal cooling can enhance the SFR density even at $z \gtrsim 6$ by $\sim 20 - 30\%$. This is because the gas density becomes higher and temperature becomes lower

(see Figure 5c) by responding to the enhanced cooling rate by metals.

In summary, we consider that our study serves to demonstrate the importance of metal enrichment and metal cooling in galaxy formation, beyond our original motivation to perform a simple numerical study. Our study highlights the role of metals at low- z and high- z to enhance the star formation in the Universe, and demonstrates that the metals increase the SF efficiency in the star-forming ISM, as well as enabling more IGM to accrete onto galaxies and fuel star formation. We expect that metal cooling would also alter some of the galaxy properties such as the mass-metallicity relationship (e.g., Tremonti et al. 2004) and specific SFR (e.g.,

Noeske et al. 2007). We plan to investigate these issues in the future, as well as alternative models for star formation and feedback.

ACKNOWLEDGEMENTS

We thank V. Springel for allowing us to use the updated version of GADGET-2 code for our study, and for useful comments on the manuscript. KN is grateful for the hospitality of Institute for the Physics and Mathematics of the Universe, University of Tokyo, where part of this work was done. We are also grateful to the anonymous referee for constructive comments which improved this paper. This research was supported in part by the National Aeronautics and Space Administration under Grant/Cooperative Agreement No. NNX08AE57A issued by the Nevada NASA EPSCoR program, by the National Science Foundation through TeraGrid resources provided by the San Diego Supercomputer Center (SDSC), and by the President's Infrastructure Award at UNLV. The simulations were performed at the UNLV Cosmology Computing Cluster and the Datastar at SDSC.

REFERENCES

- Anders E., Grevesse N., 1989, *GeCoA*, 53, 197
- Ascasibar Y., Yepes G., Gottlöber S., Müller V., 2002, *A&A*, 387, 396
- Barnes J., Hut P., 1986, *Nature*, 324, 446
- Bessell M. S., Sutherland R. S., Ruan K., 1991, *ApJL*, 383, L71
- Burles S., Nollett K. M., Turner M. S., 2001, *ApJL*, 552, L1
- Cen R., 1992, *ApJS*, 78, 341
- Cen R., Nagamine K., Ostriker J. P., 2005, *ApJ*, 635, 86
- Cen R., Ostriker J. P., 1993, *ApJ*, 417, 415
- Cen R., Ostriker J. P., 1999, *ApJL*, 519, L109
- Davé R., Cen R., Ostriker J. P., Bryan G. L., Hernquist L., Katz N., Weinberg D. H., Norman M. L., O'Shea B., 2001, *ApJ*, 552, 473
- Davé R., Hernquist L., Katz N., Weinberg D. H., 1999, *ApJ*, 511, 521
- Davé R., Oppenheimer B. D., 2007, *MNRAS*, 374, 427
- Efstathiou G., 1992, *MNRAS*, 256, 43P
- Erb D. K., Steidel C. C., Shapley A. E., Pettini M., Reddy N. A., Adelberger K. L., 2006, *ApJ*, 646, 107
- Finlator K., Davé R., 2008, *MNRAS*, 385, 2181
- Finlator K., Davé R., Oppenheimer B. D., 2007, *MNRAS*, 376, 1861
- Finlator K., Davé R., Papovich C., Hernquist L., 2006, *ApJ*, 639, 672
- Geha M., Blanton M. R., Masjedi M., West A. A., 2006, *ApJ*, 653, 240
- Gnedin N. Y., 2000, *ApJ*, 542, 535
- Governato F., Mayer L., Wadsley J., Gardner J. P., Willman B., Hayashi E., Quinn T., Stadel J., Lake G., 2004, *ApJ*, 607, 688
- Governato F., Willman B., Mayer L., Brooks A., Stinson G., Valenzuela O., Wadsley J., Quinn T., 2007, *MNRAS*, 374, 1479
- Haardt F., Madau P., 1996, *ApJ*, 461, 20
- Hernquist L., Springel V., 2003, *MNRAS*, 341, 1253
- Hockney R. W., Eastwood J. W., 1988, *Computer simulation using particles*. Bristol: Hilger, 1988
- Hoeft M., Yepes G., Gottlöber S., Springel V., 2006, *MNRAS*, 371, 401
- Hui L., Gnedin N. Y., 1997, *MNRAS*, 292, 27
- Katz N., Hernquist L., Weinberg D. H., 1992, *ApJL*, 399, L109
- Katz N., Weinberg D. H., Hernquist L., 1996, *ApJS*, 105, 19
- Kawata D., Gibson B. K., 2003, *MNRAS*, 340, 908
- Kennicutt Jr. R. C., 1998a, *ARA&A*, 36, 189
- Kennicutt Jr. R. C., 1998b, *ApJ*, 498, 541
- Kereš D., Katz N., Weinberg D. H., Davé R., 2005, *MNRAS*, 363, 2
- Kobayashi C., 2004, *MNRAS*, 347, 740
- Kobayashi C., Springel V., White S. D. M., 2007, *MNRAS*, 376, 1465
- Kravtsov A. V., 2003, *ApJL*, 590, L1
- Lia C., Portinari L., Carraro G., 2002, *MNRAS*, 330, 821
- Marri S., White S. D. M., 2003, *MNRAS*, 345, 561
- Martin C. L., 2005, *ApJ*, 621, 227
- Martin C. L., 2006, *ApJ*, 647, 222
- Martínez-Serrano F. J., Serna A., Domínguez-Tenreiro R., Mollá M., 2008, *ArXiv e-prints*, 804
- McKee C. F., Ostriker E. C., 2007, *ARA&A*, 45, 565
- Murali C., Katz N., Hernquist L., Weinberg D. H., Davé R., 2002, *ApJ*, 571, 1
- Murray N., Quataert E., Thompson T. A., 2005, *ApJ*, 618, 569
- Nagamine K., 2002, *ApJ*, 564, 73
- Nagamine K., Cen R., Hernquist L., Ostriker J. P., Springel V., 2005a, *ApJ*, 627, 608
- Nagamine K., Cen R., Hernquist L., Ostriker J. P., Springel V., 2005b, *ApJ*, 618, 23
- Nagamine K., Cen R., Ostriker J. P., 2000, *ApJ*, 541, 25
- Nagamine K., Fukugita M., Cen R., Ostriker J. P., 2001a, *MNRAS*, 327, L10
- Nagamine K., Fukugita M., Cen R., Ostriker J. P., 2001b, *ApJ*, 558, 497
- Nagamine K., Ostriker J. P., Fukugita M., Cen R., 2006, *ApJ*, 653, 881
- Nagamine K., Springel V., Hernquist L., 2004, *MNRAS*, 348, 421
- Nagamine K., Springel V., Hernquist L., Machacek M., 2004, *MNRAS*, 350, 385
- Noeske K. G., Faber S. M., Weiner B. J., Koo D. C., Primack J. R., Dekel A., Papovich C., Conselice C. J., Le Floch E., Rieke G. H., Coil A. L., Lotz J. M., Somerville R. S., Bundy K., 2007, *ApJL*, 660, L47
- Okamoto T., Gao L., Theuns T., 2008, *MNRAS*, 390, 920
- Oppenheimer B. D., Davé R., 2006, *MNRAS*, 373, 1265
- Pearce F. R., Jenkins A., Frenk C. S., White S. D. M., Thomas P. A., Couchman H. M. P., Peacock J. A., Efstathiou G., 2001, *MNRAS*, 326, 649
- Pontzen A., Governato F., Pettini M., Booth C. M., Stinson G., Wadsley J., Brooks A., Quinn T., Haehnelt M., 2008, *MNRAS*, 390, 1349
- Quinn T., Katz N., Efstathiou G., 1996, *MNRAS*, 278, L49
- Recchi S., Matteucci F., D'Ercole A., 2001, *MNRAS*, 322, 800

- Rees M. J., 1986, MNRAS, 218, 25P
- Rees M. J., Ostriker J. P., 1977, MNRAS, 179, 541
- Robertson B., Yoshida N., Springel V., Hernquist L., 2004, ApJ, 606, 32
- Scannapieco C., Tissera P. B., White S. D. M., Springel V., 2005, MNRAS, 364, 552
- Scannapieco C., Tissera P. B., White S. D. M., Springel V., 2006, MNRAS, 371, 1125
- Spergel D. N., Verde L., Peiris H. V., Komatsu E., Nolte M. R., Bennett C. L., Halpern M., Hinshaw G., Jarosik N., Kogut A., Limon M., Meyer S. S., Page L., Tucker G. S., Weiland J. L., Wollack E., Wright E. L., 2003, ApJS, 148, 175
- Springel V., 2005, MNRAS, 364, 1105
- Springel V., Hernquist L., 2002, MNRAS, 333, 649
- Springel V., Hernquist L., 2003a, MNRAS, 339, 289
- Springel V., Hernquist L., 2003b, MNRAS, 339, 312
- Springel V., White S. D. M., Tormen G., Kauffmann G., 2001, MNRAS, 328, 726
- Sutherland R. S., Dopita M. A., 1993, ApJS, 88, 253
- Tasker E. J., Bryan G. L., 2006, ApJL, 642, L5
- Tornatore L., Borgani S., Dolag K., Matteucci F., 2007, MNRAS, 382, 1050
- Tremonti C. A., Heckman T. M., Kauffmann G., Brinchmann J., Charlot S., White S. D. M., Seibert M., Peng E. W., Schlegel D. J., Uomoto A., Fukugita M., Brinkmann J., 2004, ApJ, 613, 898
- Weinberg D. H., Davé R., Katz N., Hernquist L., 2004, ApJ, 601, 1
- Weinberg D. H., Hernquist L., Katz N., 2002, ApJ, 571, 15
- Wheeler J. C., Sneden C., Truran Jr. J. W., 1989, ARA&A, 27, 279
- White S. D. M., Rees M. J., 1978, MNRAS, 183, 341